Heterogeneous Catalysis

International Edition: DOI: 10.1002/anie.201603204
German Edition: DOI: 10.1002/ange.201603204

Operando Synchrotron X-ray Powder Diffraction and Modulated-Excitation Infrared Spectroscopy Elucidate the CO_2 Promotion on a Commercial Methanol Synthesis Catalyst

*Oliver Martin, Cecilia Mondelli, Antonio Cervellino, Davide Ferri, Daniel Curulla-Ferré, and Javier Pérez-Ramírez**

Abstract: *Optimal amounts of CO_2 are added to syngas to boost the methanol synthesis rate on Cu-ZnO-Al_2O_3 in the industrial process. The reason for CO_2 promotion is not sufficiently understood at the particle level due to the catalyst complexity and the high demands of characterization under true reaction conditions. Herein, we applied operando synchrotron X-ray powder diffraction and modulated-excitation infrared spectroscopy on a commercial catalyst to gain insights into its morphology and surface chemistry. These studies unveiled that Cu and ZnO agglomerate and ZnO particles flatten under CO/H_2 and/or CO_2/H_2. Under the optimal CO/CO_2/H_2 mixture, sintering is prevented and ZnO crystals adopt an elongated shape due to the minimal presence of the H_2O byproduct, enhancing the water-gas shift activity and thus the methanol production. Our results provide a rationale to the CO_2 promotion emphasizing the importance of advanced analytical methods to establish structure–performance relations in heterogeneous catalysis.*

While methanol (MeOH) synthesis via CO_2 hydrogenation might become practically relevant in the future thanks to advances in catalyst design,[1] this basic chemical is currently industrially produced from syngas ($CO + 2\,H_2 \rightleftarrows CH_3OH$) over a Cu-ZnO-$Al_2O_3$ catalyst at elevated pressures (5.0–10.0 MPa) and temperatures (473–573 K).[2] Small amounts of CO_2 (ca. 3 vol.%) are added to the syngas leading to a 3–6 times enhancement of the MeOH formation rate.[3] It is widely accepted that the so-called "CO_2 promotion" is related to the transformation of CO into CO_2 via the water-gas shift (WGS) reaction ($CO + H_2O \rightleftarrows CO_2 + H_2$) and its subsequent hydrogenation to MeOH ($CO_2 + 3\,H_2 \rightleftarrows CH_3OH + H_2O$).[4] The latter is much faster than the hydrogenation of CO but strongly limited by thermodynamics and product inhibition by H_2O at high CO_2 concentrations resulting in the typical volcano plot shown in Figure 1 (described later). Klier et al.[3a] speculated that an optimal oxidation state of Cu, i.e., partially oxidized, correlates with the top of the curve. This hypothesis has never been confirmed for commercial catalysts under reaction conditions and neglects the essential role of ZnO uncovered in the CO_2 promotion.[3b] Multiple studies have revealed that zinc oxide strongly influences the CO_2 hydrogenation, acting as a structural and electronic promoter for Cu.[5] As indicated recently, this reaction appears to be favored over the reverse water-gas shift (RWGS) on a composite obtained by mechanical mixing of large particles of Cu and Al_2O_3 with ZnO in a plate-like shape with respect to the case of a mixture containing rod-like ZnO crystallites,[5d] based on the stronger electronic interactions between ZnO and Cu in the former catalyst. However, the relevance of the structure–function relationships derived in these works is limited by the use of model materials and/or ex situ characterization. Indeed, it has conclusively been demonstrated that only in situ and operando methods enable the detection of dynamic changes in the structure of heterogeneous catalysts at work which may be linked to the reaction mechanism.[6] As a first step in this direction, operando X-ray absorption spectroscopy (XAS), synchrotron X-ray powder diffraction (SXRPD), and in situ transmission electron microscopy (TEM) at (sub)ambient pressure have been applied over Cu supported on ZnO, evidencing that copper forms disc-like particles wetted by Zn atoms under strongly reducing gas mixtures (CO/H_2) and spherical particles in the presence of H_2O and/or CO_2.[7] Similar results were also obtained under WGS conditions while the effect of the ZnO morphology has not been assessed even though interactions between the Cu and ZnO phases were verified.[8] In addition, key intermediates of CO_2 hydrogenation could be detected on an industrial Cu-ZnO-Al_2O_3 catalyst using in situ diffuse reflectance infrared Fourier transform spectroscopy (DRIFTS) at 3.0 MPa and 373–473 K.[9] Still, these analyses have not assessed structural and mechanistic aspects under industrially relevant pressures and temperatures to explain the CO_2 promotion for a multicomponent commercial catalyst.

Consequently, we investigated for the first time a commercial Cu-ZnO-Al_2O_3 material by operando SXRPD during hydrogenation of CO, CO_2, and CO/CO_2 to MeOH at 543 K and 5.0 MPa, using the composition leading to the maximal MeOH formation rate for the mixed syngas feed, to correlate changes of the particle morphology with the reaction rates. We derived mass distributions of the Cu and ZnO particles on the basis of their dimensions applying a size- and shape-

[*] Dr. O. Martin, Dr. C. Mondelli, Prof. J. Pérez-Ramírez
ETH Zurich, Department of Chemistry and Applied Biosciences,
Institute for Chemical and Bioengineering
Vladimir-Prelog-Weg 1, 8093 Zurich (Switzerland)
E-mail: jpr@chem.ethz.ch
Dr. A. Cervellino, Dr. D. Ferri
Paul Scherrer Institute
5232 Villigen (Switzerland)
Dr. D. Curulla-Ferré
Total Research & Technology Feluy
Zone Industrielle Feluy C, 7181 Seneffe (Belgium)

Supporting information for this article can be found under: http://dx.doi.org/10.1002/anie.201603204.

sensitive Debye function analysis (DFA).[10] This investigation uncovered morphological alterations occurring under CO/H_2 and CO_2/H_2, which differ from previous results gathered under conditions far from the industrial process. The distinct MeOH yields observed in the CO_2-promoted regime over the catalyst pretreated in CO/H_2 or CO_2/H_2 were correlated with its WGS activity evidenced by operando modulated-excitation DRIFTS (ME-DRIFTS). Under $CO/CO_2/H_2$, specific morphologies of Cu and ZnO were detected that facilitate the WGS reaction, thus identifying the structural reasons for the CO_2 promotion.

The Cu-ZnO-Al_2O_3 catalyst herein studied was supplied in pelletized form. The basic characterization of this material is summarized in Tables S1 and S2 in the Supporting Information. The fresh sample features a molar bulk ratio of Cu:Zn:Al = 6.0:2.6:1.3 (Cu:Zn:Al = 50.6:22.5:4.6 wt.%, Figure S1), a molar surface composition of Cu:Zn:Al:Mg:Ca = 6.0:5.1:1.3:1.1:0.3 (Figure S2), a Brunauer–Emmett–Teller (BET) surface area of 118 $m^2 g_{cat}^{-1}$ (Figure S3), a copper surface area of 24.0 $m^2 g_{cat}^{-1}$, crystalline Cu and ZnO particles exhibiting an average size of 4.9 and 6.4 nm, respectively, and an amorphous Al_2O_3 phase. Scanning electron microscopy-energy dispersive X-ray spectroscopy (SEM-EDXS) uncovered copper-, zinc-, aluminum-, and carbon-rich regions, indicating the heterogeneous composition of the material at the μm scale (Figure S4). The MeOH space–time yield measured over this catalyst in a fixed-bed reactor set-up described elsewhere[4d] exhibits the characteristic volcano-like trend upon stepwise replacing CO by CO_2 in the feed gas (Figure 1) with a maximum for 2.4 vol.% of CO_2.

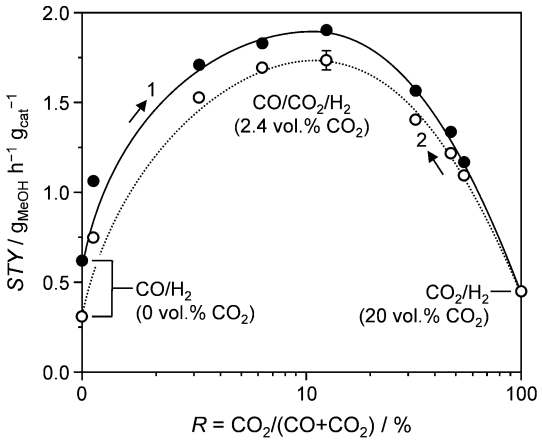

Figure 1. Methanol space–time yield (*STY*) as a function of the feed CO_2 concentration (*R*) over Cu-ZnO-Al_2O_3 upon step-wise increasing the CO_2 concentration in a CO/H_2 feed (1, solid circles) and subsequently increasing the CO concentration in a CO_2/H_2 feed (2, open circles), displaying the typical volcano-type and hysteresis behavior. For the sake of clarity, the error bar is shown for a single data point. Conditions: T = 543 K, P = 5.0 MPa, molar H_2:CO_x = 4:1, and gas hourly space velocity (*GHSV*) = 15 000 h^{-1}.

Aiming at explaining this intriguing and long-debated behavior, we designed a home-made operando cell to conduct synchrotron-based XRPD investigations in Debye–Scherrer geometry under the same reaction conditions in order to follow the changes of the crystalline Cu and ZnO phases at the extremes of the volcano (CO/H_2 and CO_2/H_2) and under the optimal gas mixture ($CO/CO_2/H_2$). The methodology of this structural analysis is shown and explained in Figure 2. Briefly, a fused-silica capillary fixed-bed reactor was housed in a heating block enabling the detection of the diffracted beams and connected to a gas feeding system. The composition of the gas at the reactor outlet was analyzed by an online mass spectrometer. The catalyst was initially exposed to CO/H_2 or CO_2/H_2 (Figure 3a, top and middle, respectively) at 5.0 MPa, 543 K, and 15 000 h^{-1}. The final MeOH concentration upon CO hydrogenation was ca. 50% of that during CO_2 hydrogenation (Figure 3a, top and middle, respectively). The concentrations of the gas components in the operando studies indicated similar reaction rates as previously measured for this catalyst.[4d] The SXRPD patterns collected during the catalytic runs (Figure S6) were matched through atomistic cluster simulations of the standard crystalline phases of Cu, Zn, and their oxides. Total scattering methods such as the DFA[10a] were applied as they enable a more effective detection of subnanometer-sized particles and of their shapes with respect to classical approaches like profile analysis,[10b,c,d] which is given in Table S3 for comparison. The diffractograms unveiled that the copper particles did not change their

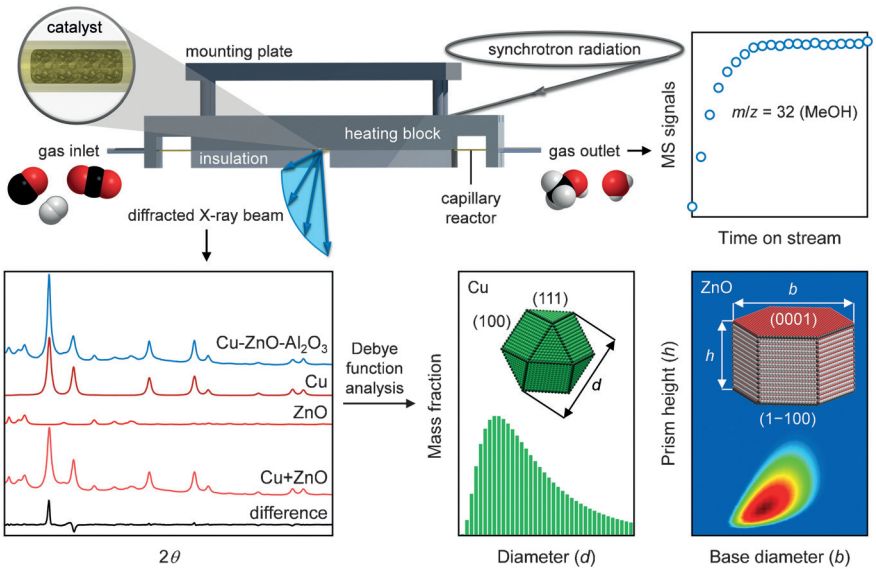

Figure 2. Operando SXRPD experiment at the synchrotron beamline. Diffraction patterns (bottom left) are collected by shining the X-ray beam onto a capillary fixed-bed reactor (top left) where the reaction takes place over Cu-ZnO-Al_2O_3 under industrial conditions of temperature, pressure, and space velocity, while the reactor outlet gas mixture is analyzed online by a mass spectrometer (top right). The measured SXRPD data (blue) are processed (red) by applying a Debye function analysis to derive the mass distributions of the Cu and ZnO particles (bottom right) based on their shape and size. A photograph of the set-up is shown in Figure S5.

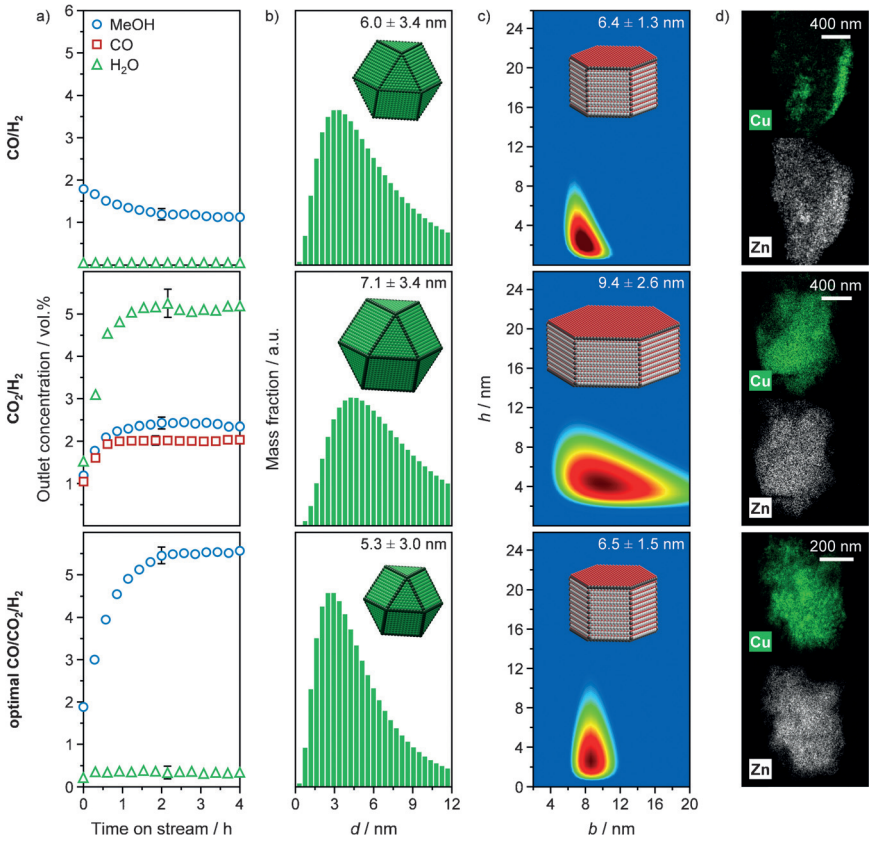

Figure 3. a) Temporal evolution of the CO, MeOH, and H_2O concentrations during the hydrogenation of CO (top), CO_2 (middle), and $CO+CO_2$ (optimal mixture, bottom). For the sake of clarity, error bars are shown for a single data point in each graph. Mass distributions of b) Cu particles of a given diameter (*d*) and of c) ZnO particles of a given base diameter (*b*) and prism height (*h*) and d) EDXS mapping of Cu and Zn for the catalyst at the end of each catalytic run. The insets in (b,c) depict models of the particles calculated based on the average dimensions.

cuboctahedral morphology upon exposure to the different gas compositions. Note that, in view of the high sensitivity of the synchrotron XRPD methodology, changes in the shape of the crystallites would have resulted in clearly detectable anisotropic broadening of the reflections. We further confirmed the preservation of the cubic symmetry of the Cu phase by conducting modulated-excitation SXRPD (ME-SXRPD) experiments (Figure S7), i.e., alternating the feed between CO/Ar and CO_2/Ar or CO/H_2 and CO_2/H_2 under the above-mentioned reaction conditions every 29 min. Such technique produces difference patterns with a higher signal-to-noise ratio, thus enabling the detection of subtle modifications of the crystallites, which may include surface changes in spite of the general bulk nature of XRPD. The retention of the shape of the Cu particles is in striking contrast to previous reports on an impregnated model Cu/ZnO catalyst, which claimed a flattening of the Cu crystallites in CO-containing atmospheres.[6] The origin of this discrepancy likely is the 10-times lower Cu loading of that material with respect to our commercial bulk system and the application of (sub)ambient pressure during its analysis by SXRPD, XAS, and TEM. On the other hand, density functional theory (DFT) calculations exploring the impact of pressure on the morphology of supported metal nanoparticles[11] corroborate the spherical shape evidenced at 5.0 MPa.

In spite of the unaltered morphology, the average size of Cu particles increased from 4.9 (Table S1) to 6.0 and 7.1 nm under CO/H_2 and CO_2/H_2, respectively (Figure 3b, top and middle). In the former case, sintering was gradual (Figure S6b) and likely favored by the segregation of Cu from ZnO, indicated by energy-dispersive X-ray spectroscopy (EDXS) (Figures 3d, top, and S8), while it was rapid (Figure S6d) and possibly induced by the presence of the H_2O byproduct in the latter environment (Figure 3a, middle).[2] Since CO_2 hydrogenation is the main reaction pathway to MeOH from mixed syngas,[4a–d] we evaluated how the different sizes of the Cu particles induced by CO_2/H_2 and CO/H_2 affect the activity of this reaction (Figures 4a and c, respectively). MeOH was formed over the catalyst pretreated in CO/H_2 in a moderately larger amount than over a sample exposed to CO_2/H_2 (2.55 vs. 2.40 vol.%, respectively). In both tests, the Cu particles experienced a further growth, but they remained smaller (6.7 vs. 7.8 nm) in the sample pretreated in CO/H_2. These observations are in line with the slightly higher CO_2 hydrogenation turnover frequency over Cu/ZnO catalysts featuring a higher Cu dispersion ($d=5$–36 nm, determined ex situ).[12] A minor loss in crystallinity of the Cu phase was detected in ME-SXRPD upon exchanging CO_2 by CO in H_2 or Ar (Figure S7b and c, respectively), pointing to the surface oxidation of Cu, which was also observed by Auger electron spectroscopy (Figure S2c). However, the reversible nature of this change does not explain the different catalyst activity after the distinct pretreatments discussed above.

In addition, the mass distributions of the ZnO particles were calculated from the SXRPD patterns revealing a hexagonal prism-like morphology. The average size (6.4 nm) did not change under the CO/H_2 atmosphere (Figure 3c, top), but largely increased (9.4 nm) upon CO_2 hydrogenation. A preferential growth of the hexagonal base diameter was determined, resulting in flatter ZnO crystallites (Figure 3c, middle). Likely due to the poor contrast between Cu and ZnO, such structural alterations were not visualized by transmission electron microscopy (TEM) of the used materials (Figure S9). Based on the work by Tsang et al.[5d] on mechanically-mixed $Cu/ZnO/Al_2O_3$ catalysts, it was expected that the different proportion between the base and the height of the prisms of ZnO would impact the CO_2 hydrogenation rate since the selectivity to MeOH from CO_2/H_2 was higher over plate-like rather than rod-like particles. That difference was explained by an improved electronic interaction with Cu

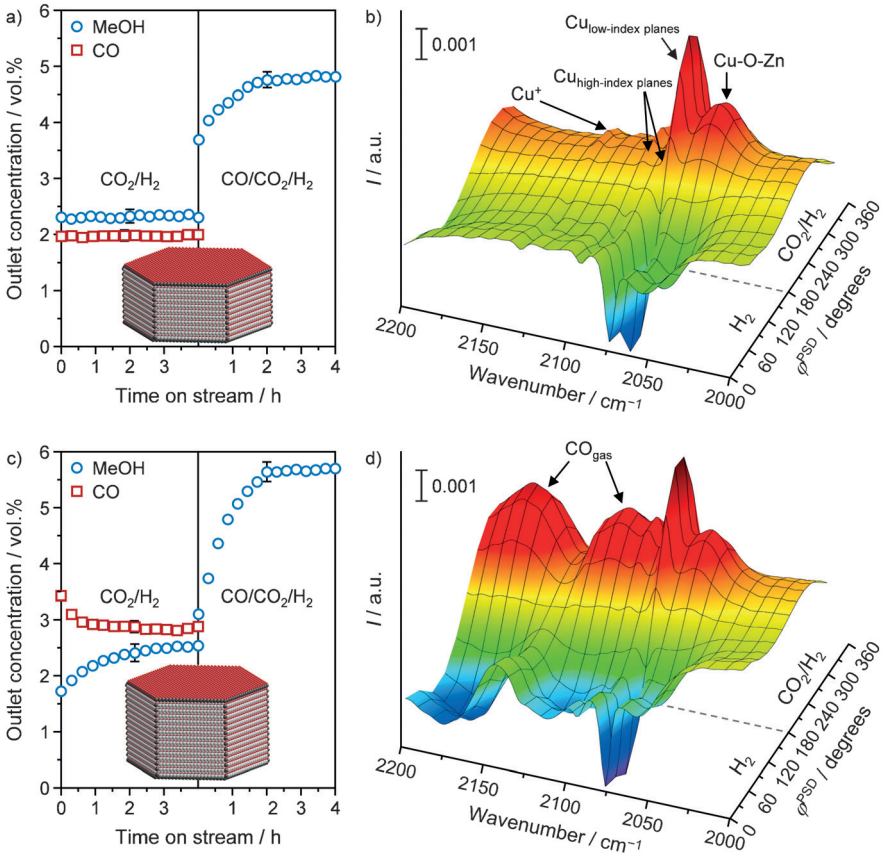

Figure 4. a,c) Temporal evolution of the CO and MeOH concentrations during hydrogenation of CO_2 and $CO+CO_2$ (optimal mixture) over Cu-ZnO-Al_2O_3 pretreated for 4 h in a) CO_2/H_2 and c) CO/H_2. For the sake of clarity, error bars are shown for a single data point in each graph. b,d) Phase-resolved DRIFT spectra obtained from a modulated-excitation experiment in which pulses ($t=20$ min) of H_2 and CO_2/H_2 were alternatively admitted to the catalyst after a 4-h pretreatment in b) CO_2/H_2 and d) CO/H_2. Arrows in (b,d) mark the bands of gaseous CO and CO adsorbed on distinct surface sites. The corresponding MS signals are depicted in Figures S10e and f. Conditions for the DRIFTS experiments: $T=373$ K, $P=5.0$ MPa, molar $H_2:CO_2=4:1$, and $GHSV=30000$ h^{-1}.

in the former case, originating from an enhanced exhibition of polar facets (e.g., (0001)). Although our selectivity patterns upon CO_2 hydrogenation after the CO_2/H_2 and CO/H_2 pretreatments (Figures 4a,c) agree well with Ref. [5d], the difference in MeOH concentration was rather low in our study (2.55 vs. 2.40 vol.%). Consequently, we propose that the concomitant RWGS reaction is more sensitive to the ZnO morphology, corroborating the strong inhibiting effect of ZnO covering the Cu phase for this reaction[4d,13] and the much higher concentration of CO measured after the CO/H_2 pretreatment (2.81 vs. 1.97 vol.%).

In order to correlate the alterations at the particle level with the surface chemistry, we conducted operando ME-DRIFTS investigations upon CO_2 hydrogenation after pretreatment of the catalyst in CO_2/H_2 and CO/H_2 (Figures 4b,d, and S10), in analogy to the SXRPD experiments. The gas feed composition was exchanged every 20 min between CO_2/H_2 and H_2 at 373 K and 5.0 MPa. The lower reaction temperature was selected to prevent an excessive CO production, since intense bands of gaseous CO would mask the signals related to adsorbed CO species (Figure S11). As described in greater detail in the Supporting Information, the spectra obtained featured signals attributed to CO adsorbed on low-index (e.g., (111), 2058 and 2077 cm^{-1}) and high-index faces of Cu^0 (e.g., (755), 2092 cm^{-1}), as well as on Cu^+ sites (2129 cm^{-1})[9] irrespective of the pretreatment. Since the RWGS reaction predominantly occurs over the low-index Cu planes, the Cu particle size may not have a significant impact on the reaction rate. Still, CO adsorbed on Cu sites next to ZnO (2058 cm^{-1}) was identified in both experiments, which hints to the sensitivity of this reaction to the interaction of Cu with the ZnO particles and, in turn, the size and shape of the latter. This evidence correlates with the enhancement of the CO_2 hydrogenation and RWGS over Cu_{29} clusters on polar ZnO surfaces compared to pure Cu.[14] Additional weak features were detected in both ME-DRIFTS experiments (Figures S10b and d). Bands at 1932 and 1910 cm^{-1} have been associated with CO adsorbed on $CuZn_x$ alloys, which some studies considered as the active sites in CO_2 hydrogenation.[5e,g,7] The changes of the ZnO and Cu reflections in the ME-SXRPD experiment (Figure S7b) could be compatible with the reversible formation of such species in line with their observation on the surface of lab-prepared Cu-ZnO-Al_2O_3 by in situ Auger electron spectroscopy.[5g] However, their contribution to the RWGS reaction appears to be minor in view of the much stronger intensity of the infrared signals of CO adsorbed on the other Cu sites. Bands of gaseous CO were absent for the sample pretreated in CO_2/H_2, evidencing its hindered desorption when platelet-like structures of ZnO are formed (Figure 4b). In contrast, prominent and modulating signals of gaseous CO were detected in the measurement conducted after the CO/H_2 pretreatment (Figure 4d), supporting the higher RWGS activity of a sample in which Cu likely interacts more with non-polar facets of ZnO (e.g., (1−100), Figure 4c). We propose that, according to the principle of microscopic reversibility,[15] the WGS activity relates to the particle structure similarly to the RWGS activity. This emphasizes the importance of the derived correlations for CO_2-promoted MeOH synthesis explaining why Cu-ZnO-Al_2O_3 catalysts with large zinc contents do not catalyze the WGS and, hence, do not feature CO_2 promotion.[4d] In line with the catalytic data, the pretreatment does not affect the mechanism of CO_2 hydrogenation (Figures S10a–d). In this respect, the phase-resolved analysis (Figures S10b and d) uncovered two important aspects. Firstly, the unperturbed intensity of formate bands during the modulation suggests that such species are spectators rather than reaction intermediates, in

contrast to recent kinetic models[5e,9,16] but in agreement with studies proposing a carboxyl (COOH*)-based route.[17] Secondly, the detection of bands assigned to methoxy species on Cu and ZnO sites emphasizes the necessity to consider both catalyst components in future molecular studies.

In order to unravel the structure of Cu and ZnO in the promotional regime, the catalyst was exposed to mixed syngas ($CO/CO_2/H_2$) with the optimal CO_2 content ($R = CO_2/(CO + CO_2) = 12\,\%$, 2.4 vol.% CO_2, Figure 1). The final MeOH concentration in this experiment (Figure 3a, bottom) was ca. 1.6-times larger than the sum of the MeOH concentrations expected for the amounts of CO and CO_2 in the feed, in line with the activity enhancement observed in Figure 1. Under this condition, the Cu and ZnO particles substantially retained their original size (5.3 and 6.4 nm, respectively, Figure 3b and c, bottom) and relative distribution (Figure 3d, bottom). It is worth noting that the H_2O produced via CO_2 hydrogenation was almost fully consumed by the WGS reaction (Figure 3a, bottom), which might account for the minimized sintering of Cu and ZnO. Nevertheless, a slight elongation of the ZnO crystallites along the (0001) axis became evident. To shed light on the impact of the ZnO morphology on the CO_2 promotion, we applied $CO/CO_2/H_2$ gas mixtures over samples pretreated in CO_2/H_2 or CO/H_2 (Figures 4a,c, respectively) and thus featuring different ZnO particles, as described above. The extent of promotion was ca. 20% lower after the former treatment, in line with the hysteresis behavior shown in Figure 1, i.e., the promotional effect of CO_2 is still present but less pronounced when starting from a CO_2/H_2 feed with respect to starting from a CO/H_2 feed. Ex situ characterization has excluded that this effect is associated with an irreversible deactivation of the catalyst, e.g., continuous sintering upon the cycle.[3b] Interestingly, the CO_2 hydrogenation rate was similar after the pretreatments in CO_2/H_2 or CO/H_2 (Figure 4a,c, respectively), substantiating that this reaction is not the limiting step under the promotional regime. Additionally, it is evident that CO_2 promotion was suppressed to a comparable extent to the RWGS reaction in samples with platelet-like ZnO crystallites (Figure 4a). Previous DFT studies on a Cu surface did not indicate optimal turnover frequencies nor coverages of intermediates under mixed syngas conditions.[16] We therefore explain the top of the cycle (Figure 1) mainly as a result of the depleted contacts between Cu particles and polar ZnO facets due to the elongation of the latter along the hexagonal prism axis (0001) under the optimal $CO/CO_2/H_2$ mixture boosting the WGS and consequently the CO_2 promotion.

In conclusion, our study established correlations between the Cu and ZnO particle size and morphology, the reaction mechanism, and the activity of a commercial Cu-ZnO-Al_2O_3 catalyst upon methanol synthesis under various gas compositions and industrial conditions. Operando SXRPD elucidated that Cu particles retained their cuboctahedral shape but sintered under CO/H_2 and CO_2/H_2. This phenomenon was associated with the segregation of Cu from ZnO upon CO hydrogenation and with the presence of H_2O upon CO_2 hydrogenation. With respect to the hexagonal ZnO particles, a CO/H_2 atmosphere did not provoke significant alterations but growth and formation of platelet-like morphologies were observed under CO_2/H_2. Since CO_2 hydrogenation was only slightly improved over smaller Cu particles and was insensitive to the morphology of ZnO, we deduced that this reaction cannot become a limiting step for the promotional effect. In the $CO/CO_2/H_2$ mixture with the optimal CO_2 concentration, the low amount of H_2O formed prevented Cu and ZnO sintering. Moreover, the ZnO prism-like crystallites preferentially elongated along their hexagonal axis. ME-DRIFTS during reaction evidenced a strong suppression of the RWGS in catalyst samples containing platelet-like ZnO particles. The higher amount of polar facets in these structures leads to enhanced electronic interactions with Cu, which inhibit the active sites on the latter. In contrast, the preferred elongation of ZnO under the optimal gas mixture augmented the fraction of non-polar facets exposed, boosting the WGS reaction and, thus, the MeOH formation from CO_2. These findings rationalize the promotional effect and indicate that the best catalyst structure for CO_2-promoted MeOH synthesis comprises small Cu particles in contact with rod-like ZnO crystallites, preferably stabilized by structural promoters.

Experimental Section

The Cu-ZnO-Al_2O_3 catalyst was purchased in pelletized form (5.5 mm in diameter and 3.6 mm in height) from Alfa Aesar (product No. 45776). The bulk and surface composition, the copper surface area, and the porosity and structure of the fresh catalyst were studied by X-ray fluorescence spectroscopy, X-ray photoelectron spectroscopy, temperature-programmed reduction with H_2 after oxidation with N_2O, N_2 sorption at 77 K, and scanning (transmission) electron microscopy-energy dispersive X-ray spectroscopy. Operando synchrotron X-ray powder diffraction (SXRPD) was carried out at the X04SA-MS beamline of the Swiss Light Source (SLS) synchrotron of the Paul Scherrer Institute (PSI), Switzerland.[18] The undiluted catalyst ($W_{cat} = 50$ mg, particle size = 75–150 μm) was loaded into a custom-made capillary cell connected to a gas feeding system and a mass spectrometer, activated in a gas flow ($F_{total} = 16.5$ cm^3 STP min^{-1}) of 5 vol.% H_2 in Ar at 5.0 MPa and 543 K (2 K min^{-1}) for 30 min, and then exposed to a gas feed with a molar composition of H_2:CO:Ar (coded "CO/H_2") or H_2:CO_2:Ar (coded "CO_2/H_2") = 4:1:1.5 or H_2:CO:CO_2:Ar (coded "$CO/CO_2/H_2$") = 4:0.88:0.12:1.5 for 4 h. In certain experiments, the catalyst was additionally contacted with CO_2/H_2 or $CO/CO_2/H_2$ for 4 h after activation and exposure to CO/H_2 or CO_2/H_2. In modulated-excitation SXRPD (ME-SXRPD) studies, the activated catalyst was subjected to 10 cycles of 57 min during which the gas feed was alternated between two compositions. The beam energy was set at 22 keV for optimal penetration. Diffraction patterns were collected in the 2–120° 2θ range over 43.5 (ME-SXRPD) or 60 s (SXRPD) with a resolution of 0.0036° 2θ with the aid of the position-sensitive single-photon counting MYTHEN II detector.[19] Measured diffraction patterns were background subtracted and fitted by the Debye function analysis method[9] deriving mass fractions on the basis of the dimensions of each crystalline phase. The patterns of the known structures of Cu, Zn, and their oxides were sufficient to match all diffractograms acquired in this study, since the residual patterns were flat and stochastic (except for texture artefacts). Operando modulated-excitation diffuse reflectance infrared Fourier transform spectroscopy (ME-DRIFTS) investigations were performed using the same reactor set-up employed for the SXRPD analysis but replacing the capillary cell by a high-pressure diffuse reflectance reaction chamber (Harrick) placed into a Bruker Equinox 55 spectrometer equipped with a liquid-N_2-cooled MCT detector. The activated catalyst ($W_{cat} = 25$ mg, 1:1 dilution with Si (Acros Organics, 99%), particle size = 75–150 μm) was pretreated in

CO/H_2 or CO_2/H_2 at 543 K and 5.0 MPa for 4 h and then cooled to 373 K in an Ar flow. After complete purging, the gas flow was alternated between molar H_2:Ar = 4:2.5 (1200 s) and H_2:CO_2:Ar = 4:1:1.5 (1200 s) 10 times. Time-resolved spectra were acquired every 60 s accumulating 200 scans in the 4000–600 cm^{-1} range (4 cm^{-1} resolution) and processed by a reported procedure to derive phase-resolved spectra.[20] Further details to these procedures are provided in the Supporting Information.

Acknowledgements

Total Research & Technology Feluy for sponsoring this research. The Scientific Center for Optical and Electron Microscopy at ETH Zurich, ScopeM, and the X04SA-Materials Science MS beamline at the Swiss Light Source (SLS) of the Paul Scherrer Institute (PSI) for granting access to their facilities. Sharon Mitchell for the electron microscopic studies. Stef Smeets for diffraction data interpretation.

Keywords: carbon dioxide chemistry · heterogeneous catalysis · methanol synthesis · operando characterization · structure–activity relationships

How to cite: *Angew. Chem. Int. Ed.* **2016**, *55*, 11031–11036
Angew. Chem. **2016**, *128*, 11197–11202

[1] a) W. Wang, S. Wang, X. Ma, J. Gong, *Chem. Soc. Rev.* **2011**, *40*, 3703–3727; b) O. Martin, A. J. Martín, C. Mondelli, S. Mitchell, T. F. Segawa, R. Hauert, C. Drouilly, D. Curulla-Ferré, J. Pérez-Ramírez, *Angew. Chem. Int. Ed.* **2016**, *55*, 6261–6265; *Angew. Chem.* **2016**, *128*, 6369–6373.

[2] J. B. Hansen, P. E. H. Nielsen, in *Handbook of Heterogeneous Catalysis*, *Vol. 6*, *2nd ed.* (Eds.: G. Ertl, H. Knözinger, F. Schüth, J. Weitkamp), Wiley-VCH, Weinheim, **2008**, pp. 2920–2949.

[3] a) K. Klier, V. Chatikavanij, R. G. Herman, G. W. Simmons, *J. Catal.* **1982**, *74*, 343–360; b) O. Martin, J. Pérez-Ramírez, *Catal. Sci. Technol.* **2013**, *3*, 3343–3352.

[4] a) Y. Zhang, Q. Sun, J. Deng, D. Wu, S. Chen, *Appl. Catal. A* **1997**, *158*, 105–120; b) A. Y. Rozovskii, G. I. Lin, *Kinet. Catal.* **1999**, *40*, 773–794; c) F. Studt, M. Behrens, E. L. Kunkes, N. Thomas, S. Zander, A. Tarasov, J. Schumann, E. Frei, J. B. Varley, F. Abild-Pedersen, J. K. Nørskov, R. Schlögl, *ChemCatChem* **2015**, *7*, 1105–1111; d) O. Martin, C. Mondelli, D. Curulla-Ferré, C. Drouilly, R. Hauert, J. Pérez-Ramírez, *ACS Catal.* **2015**, *5*, 5607–5616; e) E. L. Kunkes, F. Studt, F. Abild-Pedersen, R. Schlögl, M. Behrens, *J. Catal.* **2015**, *328*, 43–48.

[5] a) S. A. French, A. A. Sokol, S. T. Bromley, C. R. A. Catlow, S. C. Rogers, F. King, P. Sherwood, *Angew. Chem. Int. Ed.* **2001**, *40*, 4437–4440; *Angew. Chem.* **2001**, *113*, 4569–4572; b) S. Polarz, J. Strunk, V. Ischenko, M. W. E. van den Berg, O. Hinrichsen, M. Muhler, M. Driess, *Angew. Chem. Int. Ed.* **2006**, *45*, 2965–2969; *Angew. Chem.* **2006**, *118*, 3031–3035; c) I. Kasatkin, P. Kurr, B. Kniep, A. Trunschke, R. Schlögl, *Angew. Chem. Int. Ed.* **2007**, *46*, 7324–7327; *Angew. Chem.* **2007**, *119*, 7465–7468; d) F. Liao, Y. Huang, J. Ge, W. Zheng, K. Tedsree, P. Collier, X. Hong, S. C. Tsang, *Angew. Chem. Int. Ed.* **2011**, *50*, 2162–2165; *Angew. Chem.* **2011**, *123*, 2210–2213; e) M. Behrens, F. Studt, I. Kasatkin, S. Kühl, M. Hävecker, F. Abild-Pedersen, S. Zander, F. Girgsdies, P. Kurr, B.-L. Kniep, M. Tovar, R. W. Fischer, J. K. Nørskov, R. Schlögl, *Science* **2012**, *336*, 893–897; f) S. Zander, E. L. Kunkes, M. E. Schuster, J. Schumann, G. Weinberg, D. Teschner, N. Jacobsen, R. Schlögl, M. Behrens, *Angew. Chem. Int. Ed.* **2013**, *52*, 6536–6540; *Angew. Chem.* **2013**, *125*, 6664–6669; g) S. Kuld, C. Conradsen, P. G. Moses, I. Chorkendorff, J. Sehested, *Angew. Chem. Int. Ed.* **2014**, *53*, 5941–5945; *Angew. Chem.* **2014**, *126*, 6051–6055.

[6] a) B. M. Weckhuysen in *In-situ Characterization of Catalysts*, American Scientific, Stevenson Ranch, **2004**; b) I. E. Wachs, C. A. Roberts, *Chem. Soc. Rev.* **2010**, *39*, 5002–5017; c) G. A. Somorjai, S. K. Beaumont, S. Alayoglu, *Angew. Chem. Int. Ed.* **2011**, *50*, 10116–10129; *Angew. Chem.* **2011**, *123*, 10298–10311; d) M. A. Bañares, *Adv. Mater.* **2011**, *23*, 5293–5301; e) J. A. Rodriguez, J. C. Hanson, P. J. Chupas in *In-situ Characterization of Heterogeneous Catalysts*, *2nd ed.* (Eds.: J. A. Rodriguez, J. C. Hanson, P. J. Chupas), Wiley-VCH, Weinheim, **2013**, pp. 1–22.

[7] a) B. S. Clausen, J. Schiøtz, L. Gråbæk, C. V. Ovesen, K. W. Jacobsen, J. K. Nørskov, H. Topsøe, *Top. Catal.* **1994**, *1*, 367–376; b) J.-D. Grunwaldt, A. M. Molenbroek, N.-Y. Topsøe, H. Topsøe, B. S. Clausen, *J. Catal.* **2000**, *194*, 452–460; c) P. L. Hansen, J. B. Wagner, S. Helveg, J. R. Rostrup-Nielsen, B. S. Clausen, H. Topsøe, *Science* **2002**, *295*, 2053–2055.

[8] J. A. Rodriguez, J. C. Hanson, D. Stacchiola, S. D. Senanayake, *Phys. Chem. Chem. Phys.* **2013**, *15*, 12004–12025.

[9] S. Bailey, G. F. Froment, J. W. Snoeck, K. C. Waugh, *Catal. Lett.* **1995**, *30*, 99–111.

[10] a) A. Cervellino, R. Frison, F. Bertolotti, A. Guagliardi, *J. Appl. Crystallogr.* **2015**, *48*, 2026–2032; b) G. Cernuto, S. Galli, F. Trudu, G. M. Colonna, N. Masciocchi, A. Cervellino, A. Guagliardi, *Angew. Chem. Int. Ed.* **2011**, *50*, 10828–10833; *Angew. Chem.* **2011**, *123*, 11020–11025; c) G. Cernuto, N. Masciocchi, A. Cervellino, G. M. Colonna, A. Guagliardi, *J. Am. Chem. Soc.* **2011**, *133*, 3114–3119; d) F. Bertolotti, D. N. Dirin, M. Ibáñez, F. Krumeich, A. Cervellino, R. Frison, O. Voznyy, E. H. Sargent, M. V. Kovalenko, A. Guagliardi, N. Masciocchi, *Nat. Mater.* **2016**, DOI: 10.1038/nmat4661.

[11] P. Raybaud, C. Chizallet, C. Mager-Maury, M. Digne, H. Toulhoat, P. Sautet, *J. Catal.* **2013**, *308*, 328–340.

[12] A. Karelovic, P. Ruiz, *Catal. Sci. Technol.* **2015**, *5*, 869–881.

[13] J. Nakamura, Y. Choi, T. Fujitani, *Top. Catal.* **2003**, *22*, 277–285.

[14] Y. Yang, J. Evans, J. A. Rodriguez, M. G. White, P. Liu, *Phys. Chem. Chem. Phys.* **2010**, *12*, 9909–9917.

[15] G. N. Lewis, *Proc. Natl. Acad. Sci. USA* **1925**, *22*, 179–183.

[16] L. C. Grabow, M. Mavrikakis, *ACS Catal.* **2011**, *1*, 365–384.

[17] a) Y.-F. Zhao, Y. Yang, C. Mims, C. H. F. Peden, J. Li, D. Mei, *J. Catal.* **2011**, *281*, 199–211; b) Y. Yang, D. Mei, C. H. F. Peden, C. T. Campbell, C. A. Mims, *ACS Catal.* **2015**, *5*, 7328–7337.

[18] P. R. Willmott, D. Meister, S. J. Leake, M. Lange, A. Bergamaschi, M. Böge, M. Calvi, C. Cancellieri, N. Casati, A. Cervellino, Q. Chen, C. David, U. Flechsig, F. Gozzo, B. Henrich, S. Jäggi-Spielmann, B. Jakob, I. Kalichava, P. Karvinen, J. Krempasky, A. Lüdeke, R. Lüscher, S. Maag, C. Quitmann, M. L. Reinle-Schmitt, T. Schmidt, B. Schmitt, A. Streun, I. Vartiainen, M. Vitins, X. Wang, R. Wullschleger, *J. Synchrotron Radiat.* **2013**, *20*, 667–682.

[19] A. Bergamaschi, A. Cervellino, R. Dinapoli, F. Gozzo, B. Henrich, I. Johnson, P. Kraft, A. Mozzanica, B. Schmitt, X. Shi, *J. Synchrotron Radiat.* **2010**, *17*, 653–668.

[20] D. Baurecht, U. P. Fringeli, *Rev. Sci. Instrum.* **2001**, *72*, 3782–3792.

Received: April 1, 2016
Revised: June 22, 2016
Published online: July 7, 2016

